Vibrational Spectrum and Structure of CoO6: A Model Compound for Molecular Oxygen Reversible Binding on Cobalt Oxides and Salts; A Combined IR Matrix Isolation and Theoretical Stud...

ARTICLE *in* THE JOURNAL OF PHYSICAL CHEMISTRY A · JULY 2011

Impact Factor: 2.69 · DOI: 10.1021/jp203943x · Source: PubMed

6 AUTHORS, INCLUDING:

Asma Marzouk
Pierre and Marie Curie University - Paris 6
7 PUBLICATIONS **46** CITATIONS
SEE PROFILE

M. Esmail Alikhani
Pierre and Marie Curie University - Paris 6
107 PUBLICATIONS **1,264** CITATIONS
SEE PROFILE

THE JOURNAL OF PHYSICAL CHEMISTRY A

ARTICLE

pubs.acs.org/JPCA

Vibrational Spectrum and Structure of CoO_6: A Model Compound for Molecular Oxygen Reversible Binding on Cobalt Oxides and Salts; A Combined IR Matrix Isolation and Theoretical Study

Asma Marzouk,[†,‡] Delphine Danset,[†,‡] Ming Fei Zhou,[§] Yu Gong,[§] Mohammad E. Alikhani,[*,†,‡] and Laurent Manceron[*,†,‡]

[†]UPMC Univ. Paris 06, UMR 7075, Laboratoire de Dynamique, Interactions et Réactivité (LADIR), F-75005, Paris, France

[‡]CNRS, UMR 7075, Laboratoire de Dynamique, Interactions et Réactivité (LADIR), F-75005, Paris, France

[§]Department of Chemistry, Fudan University, Shangaï, China

ABSTRACT: The formation and structure of a novel species, a disuperoxo-cobalt dioxide complex (CoO_6), has been investigated using matrix isolation in solid neon and argon, coupled to infrared spectroscopy and by quantum chemical methods. It is found that CoO_6 can be formed by successive complexation of cobalt dioxide by molecular oxygen without activation energy by diffusion of ground state O_2 molecules at 9K in the dark. The IR data on one combination and seven fundamentals, isotopic effects, and quantum chemical calculations are both consistent with an asymmetrical structure with two slightly nonequivalent oxygen ligands complexing a cobalt dioxide subunit. Evidence for other, metastable states is also presented, but the data are not complete. The electronic structure and formation pathway of this unique, formally +VI oxidation state, complex has been investigated using several functionals of current DFT within the broken-symmetry unrestricted formalism. It has been shown that the M06L pure local functional well reproduce the experimental observations. The ground electronic state is predicted to be an open shell $^2A''$ doublet with the quartet states above by more than 9 kcal/mol and the sextet lying even higher in energy. The ground state has a strong and complex multireference character that hinders the use of more precise multireference approaches and requires caution in the methodology to be used. The geometrical, energetic, and vibrational properties have been computed.

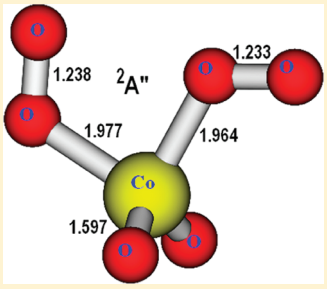

INTRODUCTION

The study of isolated oxygen complexes of transition metal molecules and their clustering processes is of fundamental interest for the understanding of the TM to oxygen coordination bonding,[1,2] but also has relevance for important applied processes, namely the search for oxygen-selective sorbents for nitrogen−oxygen air separation,[3−5] for compounds capable of reversible oxygen storage for aircraft use[6,7] or synthetic oxygen carriers related to biological systems.[8] A central question in the search for new compounds relevant to these applications is the exact structure of these O_2−Co-containing salts, the exact nature of the oxygen ligating sites,[9] the number of possible ligated oxygen molecules per Co center and its relation to the oxygen storage capacity and reversibility.[10]

Matrix isolation techniques are important tools in the experimental study of reactive molecules and to discuss formation pathways. Matrix isolation provides a unique means of investigating the formation and structures of heavy molecular transition metal oxides.[11] Chertihin and coll.[12] studied the reaction products of laser-ablated cobalt atoms and molecular oxygen isolated in solid argon. In the course of following studies of CoO_2 and $(O_2)CoO_2$ species in our laboratories,[13,14] we were able to detect the formation of another, high stoichiometry, oxygen-coordinating species, whose IR absorptions had been originally misassigned to CoO_3 in the seminal paper of Chertihin and coll.[12] After optimization of the experimental conditions, we were able to form large quantities of these species and observe new vibrational bands. The results have led us to identify this species as CoO_6, a bis-oxygen complex of cobalt dioxide. This prompted us to investigate the electronic structure and the energetics of possible formation pathways. Our goal here is to add new information relative to the formation mechanism, as well as the geometric and electronic structure of CoO_6.

EXPERIMENTAL AND COMPUTATIONAL METHODS

Experimental Details. Samples containing CoO_2 were formed by co-condensing Co vapor and dilute O_2−Ar or Ne mixtures (0.5−16% O_2/Ar or 200−2000 ppm O_2/Ne) onto one of six flat, highly polished, Rh-plated copper mirrors maintained between 3 and 15 K using a pulse-tube, closed-cycle cryogenerator (Cryomech PT405, Syracuse, U.S.A.), the experimental procedures are described in ref 15, and, after suitable photoexcitations, the CoO_2 parent molecules were formed after photochemical reactions of Co atom with

Received: April 28, 2011
Revised: July 1, 2011
Published: July 01, 2011

O_2 molecules, using IR or UV excitation, as described in refs 13 and 14.

High purity argon (Air Liquide, France; 99.995%)/neon (Air Liquide, France; 99.9995%) and $^{16}O_2$ (Air Liquide, France; 99.998%) and $^{18}O_2$ (Isotec, U.S.A., 99.0% ^{18}O) were used to prepare the O_2−Ar/Ne mixtures. To prepare scrambled oxygen ($^{16}O^{18}O$), equal quantities of $^{16}O_2$ and $^{18}O_2$ were scrambled in a Tesla discharge for approximately 10 min, the mixture then withholding 25% $^{16}O_2$, 50% $^{16}O^{18}O$, and 25% $^{18}O_2$. The gas inlet line was driven through a liquid nitrogen trap within the vacuum system thereby condensing impurities in the gas mixture and precooling it to about 77 K before reaching the mirror.

In general, after 90−120 min of deposition, infrared spectra of the resulting samples were recorded in the transmission-reflection mode between 5000 and 75 cm^{-1} using a Bruker 120 FTIR spectrometer. In the far IR region (75−600 cm^{-1}) a globar source, a Si/Mylar composite beamsplitter, a liquid He-cooled Si−B bolometer with a 4 K-cooled 660 cm^{-1} lowpass filter were used. In the mid-IR region (500−5000 cm^{-1}), a Ge/KBr beamsplitter was used along with an N_2-cooled narrow band HgCdTe photoconductor. Mid, far, and very far-infrared spectra were collected on the *same* samples. Wedged CsI and polyethylene windows were mounted on a rotatable flange separating the interferometer vacuum (5×10^{-4} mbar) from that of the cryostatic cell ($\approx 10^{-8}$ mbar). The resolution was varied from 0.05 to 0.5 cm^{-1}. Bare mirror backgrounds, recorded prior to sample deposition, and were used as references in processing the sample spectra. The spectra were subsequently subjected to baseline correction to compensate for infrared light scattering and interference patterns.

Photoexcitations were performed through a CaF_2 window mounted on the assembly. In the IR region, a 150 W globar was used, with a large parabolic collection mirror and the unfiltered irradiation power was measured around 950 mW/cm^2. High/low and band-pass filters were used and with a 4500−3900 cm^{-1} bandpass filter, photoexcitations with 40 mW/cm^2 were routinely achieved, and irradiations performed for 30−60 min. For UV−visible irradiations, an HgXe high pressure arc was used with a converging lens focusing the light on the sample and the duration of the irradiations varied from 15 to 30 min. Total UV power was measured to be about 200 mW/cm^2 for the 220−420 nm range.

Alternatively, for some experiments, narrow band (5−6 cm^{-1} line width) photoexcitations were performed using the idler beam of an OPO source operating with a BBO crystal, pumped by the third harmonic of Nd:YAG Laser (OPOTEK, QUANTEL), delivering 0.5 mJ light pulses at 20 Hz, continuously tunable in the 25000−4300 cm^{-1} range.

Computational Details. Throughout this work, the DFT method was employed using nine different functionals and two different basis sets. The chosen functionals used the generalized gradient approximation (GGA), the *meta*-generalized gradient approximation (Meta-GGA), or a hybrid functional method. The three pure GGA functionals employed in this work are BPW91, OPBE, and PBEPBE. The first functional (BPW91) contains the Becke88 exchange functional[16] and PW91 the Perdew−Wang (1991) gradient-corrected correlation functional.[17] The second one (OPBE) contains Handy's OPTX local exchange functional,[18] based on the inherent nonseparability of exchange and left-right correlation and the Perdew-Burke-Ernzerhof correlation functional (PBE).[19] Finally, the last one uses the PBE exchange and correlation functionals. The three *meta*-GGA functionals employed are TPSS-TPSS, TPSSh, and M06L. The first functional (TPSSTPSS) contains the τ-dependent gradient-corrected functional of Tao, Perdew, Staroverov, and Scuseria.[20] TPSSh is a hybrid functional formed from the TPSSTPSS functional with 10% contribution from exact exchange. M06L is the local method developed by Zhao and Truhlar.[21,22] We used also the BB95, OB95, and mPWB95 functionals, whose correlation part is the Becke's τ-dependent gradient-corrected correlation functional.[23] The exchange part of these functionals are the Becke88 (B), the Handy's OPTX, and the modified version of the Perdew−Wang 1991 ones. The last exchange functional, proposed by Adamo and Barone, is adequate to describe weak van der Waals interactions.[24]

The triple-ζ quality extended basis of Pople 6-311+G(2d)[25] and Dunning's correlation-consistent polarized valence triple-ζ basis set (Aug-cc-pVTZ)[26] were used. We decided to use at first the 6-311+G(2d) as a medium basis set with 356 primitive Gaussians, to have fast geometry optimization and assessment of the functional effect. For the vibrational study, the Aug-cc-pVTZ basis set with 817 primitive Gaussians was used for more accuracy.

All calculations were performed with the broken symmetry-unrestricted density functional theory (BS-UDFT) in order to allow static correlation effects to be described; thus, spin contamination of the wave function can be expected.[27−32] Stationary points were confirmed by calculating the normal vibrations within the harmonic approximation and by the nonexistence of imaginary frequencies. All DFT energies are corrected for the zero point vibrational energies (ZPE). The Gaussian09 program[33] was used for all calculations.

EXPERIMENTAL RESULTS

Samples were first made by co-condensation of thermally evaporated cobalt atoms and O_2−rare gas mixtures onto a highly polished mirror maintained at cryogenic temperatures, followed by IR to near UV excitation to produce the cobalt dioxide molecule.[13,14] Next, diffusion experiments were performed, raising progressively the sample temperature, while maintaining it in the dark and recording IR spectra after different annealing steps, up to 9 K for neon samples, or 30 K for argon samples. Initially, Co/Ar and O_2/Ar molar ratios were varied from 0.02 to 0.1% and 0.5 to 8%, respectively. In neon, concentrations were decreased to compensate for easier atomic and molecular diffusion. The O_2/Ne and Co/Ne molar ratios were varied from 200 to 2000 ppm and 50 to 500 ppm, respectively. The deposition temperature was varied from 9 to 12 K in argon and 3 to 6 K in neon in order to favor CoO_2 formation and improve matrix transparency. Neon samples showed a lower product yield in monocobalt species compared to argon, but no qualitative change in the chemistry of the system was observed.

Spectra taken directly after deposition in argon samples show main absorptions due to small quantities of the insertion product OCoO (945.4 cm^{-1}) and to its complex with oxygen CoO_4,[12−14] as well as Co_2O_2[12,34] the dicobalt oxide ring species, Co_2[35] and other, larger aggregates (Figure1). After near IR and UV excitation, leading to growth of the CoO_2 and Co_2O_4 absorptions,[32] molecular diffusion was promoted by progressive annealing the samples up to 30 K, which, for oxygen-rich samples, led to the strong growth of CoO_4 and, next, to the appearance of species characterized by strong absorptions near 1365.1 and 1331.3 cm^{-1}, labeled Y or CoO_y in figures of refs 13

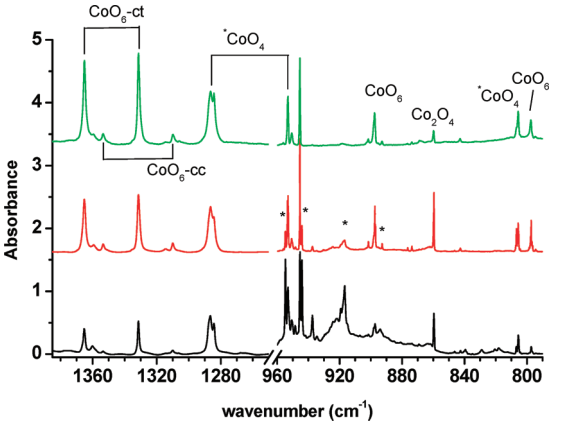

Figure 1. Infrared spectra in the 1400−750 cm^{-1} region for reaction products of matrix-isolated cobalt oxide species, as seen after formation of CoO_2, UV photoexcitation, and diffusion at 30 K, Co codeposited with $^{16}O_2$ in argon at 9 K: (a) Co/O_2/Ar = 2.5/5/1000 (ordinate scale × 3.5); (b) 2/20/1000; (c) 0.3/40/1000 (ordinate scale ×4.5). The normalization factors are chosen to have a [Co][O_2] concentration product and also normalize the CoO_2 species signal; *designates larger aggregate bands.

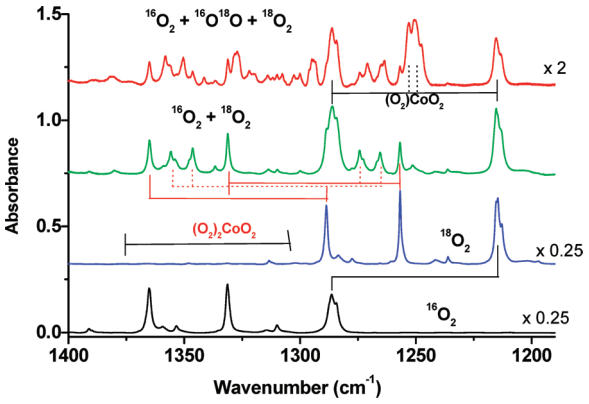

Figure 2. Isotopic study for the CoO_6 1365−1330 cm^{-1} fundamental region using different isotopic precursors. The bottom traces correspond to spectra obtained with natural or pure ^{18}O-labeled oxygen only, the third trace a O_2 + $^{18}O_2$ mixture, the top trace a O_2 + $^{16}O^{18}O$ + $^{18}O_2$ mixture.

and 14. The absorptions belonging to this species had a specific growth pattern, implying, in CoO_2-containing samples, a higher O_2 concentration dependence than the CoO_4 species (Figure 1), as these absorptions nearly double with respect to that of CoO_4 when the oxygen concentration is doubled to become the most prominent features in the spectrum.

Isotopic studies were led with $^{18}O_2$, $^{16}O_2$ + $^{18}O_2$, and $^{16}O_2$ + $^{16}O^{18}O$ + $^{18}O_2$ mixtures, showing a complex, intricate isotopic pattern, which cannot at first be easily followed as it is in part entangled with that of the strong absorption of the CoO_4 metastable state near 1286 cm^{-1} (Figure 2). This latter interference can be fortunately removed following our previous observation that the CoO_4 metastable state absorption progressively disappear if any spectrometer or background light above 2000 cm^{-1} is filtered out.

The contribution of the metastable CoO_4 can be precisely subtracted and the remaining isotopic pattern thus only pertains

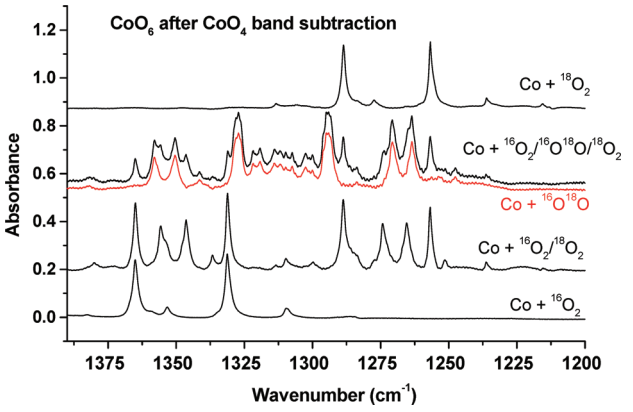

Figure 3. Isotopic study for the CoO_6 1365−1330 cm^{-1} fundamental region using different isotopic precursors. The bottom and upper traces correspond to spectra obtained with natural or pure ^{18}O-labeled oxygen only, the middle traces to O_2 + $^{18}O_2$ and O_2 + $^{16}O^{18}O$ + $^{18}O_2$ mixtures, after subtraction of spectra obtained for CoO_4. Co/O_2/Ar = 0.3/40/1000. In red: after subtraction of the Co + O_2 + $^{18}O_2$ products.

to the CoO_6 species (Figure 3). Correlated to these strong absorptions, other bands are detectable in the CoO stretching region, near 897 and 798 cm^{-1} and further down near 378, 167, and 148 cm^{-1}. All these absorptions shift with $^{18}O_2$ substitution and, for most, additional signals for $^{16}O_2$ + $^{18}O_2$ and $^{16}O_2$ + $^{16}O^{18}O$ + $^{18}O_2$ mixtures can be detected (see Table 1). For the weakest bands in the far-infrared region, however, the extra bands for the mixed isotopic species are unfortunately too weak and not clearly resolvable due to the isotopic dilution effect. Most notable is the observation, in the 1370−1260 cm^{-1} range, of two pairs of new peaks, with the $^{16}O_2$ + $^{18}O_2$ mixture, each pair framed by the absorptions observed with either $^{16}O_2$ or $^{18}O_2$ only. These four new absorptions keep the same relative intensities when the $^{16}O_2/^{18}O_2$ ratio is changed. In $^{16}O_2$ + $^{16}O^{18}O$ + $^{18}O_2$ mixtures, the spectrum in this region reveals a complex isotopic pattern with, in total, 16 new components, while only a single new peak is observed in the CoO stretching range for each fundamental.

In neon, these absorptions appear at very close frequencies, with comparable intensities and isotopic effects (for instance, the five more intense bands are observed at 1365.8, 1332.1, 899.2, and 799.3 cm^{-1}). These bands appear always correlated in our experiments, growing strongly upon diffusion and whenever large quantities of CoO_2 molecules are first formed. This species is observed only very faintly if either Co or O_2 concentration are kept low, even with high oxygen or metal contents, and is best observed in samples with comparably low cobalt and high oxygen concentrations (Figure 1). It can thus be easily distinguished from other large aggregate bands, which either grow at different rates or are light-sensitive. Note that, in contrast to other monocobalt oxide species characterized in the course of former studies (refs 13−15), this species seems very stable, growing steadily with temperature until no more precursor is present or until breakdown of the cryogenic solid and thus seems one of the end products of Co + O_2 reactions, along with Co_2O_4.[32] It is also unaffected by photolysis from IR up to 5 eV energy UV light.

Another, much weaker, set of bands can be observed in identical conditions, however. It contains three much weaker bands at 1390, 1353.3, and 1309.3 cm^{-1}. These bands behave exactly parallel to the main set, as regards growth with increasing O_2 concentration and upon molecular diffusion, but present

Table 1. Observed IR Absorptions (cm^{-1}) Observed for CoO_6 Products in Solid Ar[a]

assignment	Co + $^{16}O_2$	Co + $^{18}O_2$	Co + $^{16}O_2$ + $^{18}O_2$[b]	Co + $^{16}O^{18}O$[c]
$\nu_a + \nu_s$ OCoO	1683.4 [0.003]	1616.5		1648.0
ν O═O	1365.1 [0.91]	1288.7	1355.7	1358.1 (broader)
			1346.4	1350.4 (broader)
				1328.3
				1327.3
				1326.5
				1321.9
				1319.3
				1314.1
				1312.0
ν O═O	1353.3 [0.143]	1277.4	1336.8	
ν O═O′	1331.3 [1]	1256.8	1274.3	1309.9
			1265.5	1307.5
				1302.6
				1301.4
				1300.2
				1295.1
				1294.2
				1293.6
				1270.8 (broader)
				1263.6 (broader)
ν O═OO	1309.3 [0.134]	1236.2	1251.4	
ν_a OCoO	897.5 [0.13]	862.4		883.2
ν_s OCoO	797.8 [0.12]	758.4		774.8
ν Co-OO	377.8 [0.01]	359.4	too weak	377 (broader)
				360 (broader)
δ Co-OO ?	166.6 [0.015]	158.9	too weak	162.5 (broader)
δ Co-OO′ ?	147.6 [0.02]	139.5	too weak	144 (broader)

[a] Relative intensities in brackets. [b] Only specific additional signals are reported in addition to that observed with $^{16}O_2$ *or* $^{18}O_2$. [c] Only specific additional signals are reported in addition to that observed with $^{16}O_2$ *plus* $^{18}O_2$.

slight relative intensity changes with respect to the main set from one experiment to the next and, more important, present very slow intensity changes when samples are left in the dark. In particular, a slow decrease of the band near 1390 cm^{-1} is accompanied by a growth of the main set bands and of the 1353.3 and 1309.3 cm^{-1} set, but at different rates. This is indicative of a slow conversion process between metastable and ground states, as observed on CoO_4.

Vibrational Analysis. From the body of vibrational data and the isotopic effects gathered above, some considerations help us in inferring structural information for this species. First, judging by the isotopic effects (−32.1 and −39.4 cm^{-1} $^{16}O_2/^{18}O_2$ shifts, respectively), the two bands near 900 and 800 cm^{-1} correspond to CoO stretching modes, but of different symmetries, as observed for the CoO_2 subunit in CoO_4. The lower

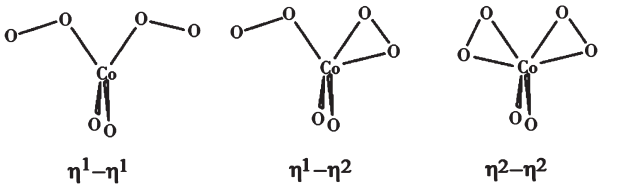

Figure 4. Three possible geometries for $OCoO(O_2)_2$.

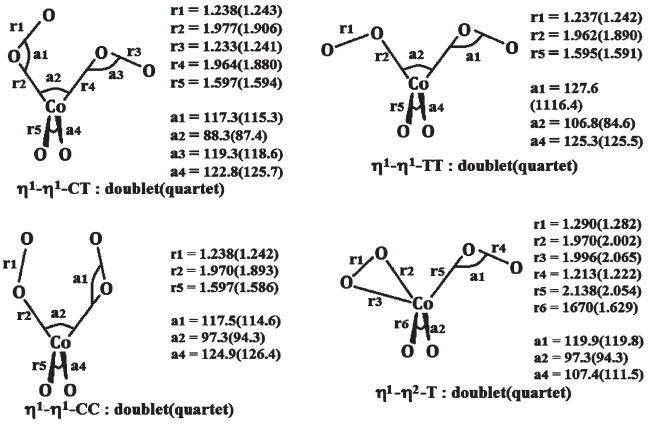

Figure 5. Optimized parameters for the four $OCoO(O_2)_2$ structures. Distances are in Å and the angles in degrees. First values are for the doublet state; quartet state values in parentheses.

band has a larger $^{16}O/^{18}O$ effect, in spite of a lower frequency, due to the larger O-atom participation for the symmetric stretching mode of a O═Co═O group with an obtuse bond angle. The position of the extra signals observed with $^{16}O^{18}O$ precursor, intermediate between the $^{16}O_2$ or $^{18}O_2$ positions, but slightly shifted above for the upper band and below for the lower one confirm this hypothesis and the existence of a bent O═Co═O group within the species.

The frequency and magnitude (about −80 cm^{-1}) of the $^{16}O_2/^{18}O_2$ shifts for the two strong, upper bands signal them unambiguously as O═O stretching modes. The addition of two ligated O_2 groups appears clearly from the concentration effect, but the isotopic data are not consistent with any symmetrical structure. A C_{2v} symmetry, $(O_2)_2CoO_2$ structure would produce only two extra peaks for $^{16}O_2$ + $^{18}O_2$ and, at most, eight others in the $^{16}O_2$ + $^{16}O^{18}O$ + $^{18}O_2$ mixture for end-on coordinated O═O groups. The presence of more than two equivalent ligated groups is not consistent with the concentration effect and would also produce different isotopic species with differing probabilities when the $^{16}O_2/^{18}O_2$ ratio is varied. Thus, the only structure consistent with the experimental data is a $(O_2)_2CoO_2$ species, in which the equivalence of the two oxygen ligands is removed. This conclusion will be further strengthened by the spectral simulations at the end of the next section.

■ ELECTRONIC STRUCTURE AND FORMATION PATHWAY OF DISUPEROXO COBALT DIOXIDE

Geometrical and Energetic Results. In relation to previous work on CoO_4,[14] we considered as starting points two structures for the cobalt dioxide in interaction with a single oxygen molecule: $OCoO(O_2)$-η^1 (in quartet state), which is first formed in the

dx.doi.org/10.1021/jp203943x |J. Phys. Chem. A 2011, 115, 9014–9021

Table 2. Energetic Parameters Obtained at the M06L/6-311+G(2d) Level[a]

state	total energy (S^2 expected value)	relative energy (cm^{-1})
$\eta_1-\eta_1$ CT ($^2A''$)	−1833.803621 (2.6)	0
$\eta1-\eta1$ CC (^2A)	−1833.803593 (2.5)	6
$\eta1-\eta1$ TT ($^2B_1$)	−1833.803073 (2.6)	120
$\eta1-\eta2$ T (^4A)	−1833.797984 (5.4)	1237
$\eta1-\eta2$ T (^2A)	−1833.795414 (3.6)	1801
$\eta1-\eta1$ CC (^4A)	−1833.789109 (3.8)	3185
$\eta1-\eta1$ CT (^4A)	−1833.786564 (3.8)	3744
$\eta1-\eta1$ TT ($^4B_1$)	−1833.785146 (3.8)	4055

[a] Total energy (in hartree) was corrected for the zero-point energy and the relative energy (in cm^{-1}) was calculated with respect to the $\eta1-\eta1$ CT ($^2A''$). The S^2 expected value for each state is reported in parentheses.

Table 3. Relative Calculated Energies (ΔE in cm^{-1}) for $^2A''-CoO_2(O_2)_2$ cis−cis, trans−trans, and cis−trans structures: the functional and basis set effects

	CC		CT		TT	
	ΔE (cm^{-1})	$\langle S^2\rangle$	ΔE (cm^{-1})	$\langle S^2\rangle$	ΔE (cm^{-1})	$\langle S^2\rangle$
			6-311+G(2d)			
TPSSTPSS	−42	2.1	0	2.1	77	2.1
TPSSh	81	2.7	0	2.7	−39	2.8
M06L	6	2.5	0	2.6	120	2.6
BPW91	−24	2.0	0	1.9	53	2.0
OPBE	222	2.2	0	2.2	−88	2.2
PBEPBE	−121	2.0	0	1.9	134	1.9
BB95	−48	1.9	0	1.8	178	1.8
OB95	549	2.1	0	2.1	9	2.1
mPWB95	−88	1.9	0	1.8	217	1,8
			Aug-cc-pVTZ basis set			
M06L	15	2.6	0	2.6	140	2.7
TPSSh	104	2.7	0	2.7	−60	2.8

$CoO_2 + O_2$ reaction, and was shown to relax next to the doublet state, $OCoO(O_2)$-η^2 (15−20 min half-life in rare gas matrices in the dark). In order to study the addition of a second oxygen molecule to $OCoO(O_2)$ species, we considered three sets of structures for CoO_6: the $\eta^1-\eta^1$, $\eta^1-\eta^2$, and $\eta^2-\eta^2$ (see Figure 4). In addition, this strategy is in line with previous works on the CuO_6 and CrO_6 compounds.[36,37] Three spin states were considered for each structure: doublet, quartet, and sextet states. To investigate all the electronic state, a systematic study was done only with the M06L/6-311+G(2d) method.

All geometrical optimizations were performed without any symmetry restriction. For each bending mode, we envisaged different conformations in relation to the OCoO plane. For example, for the mode $\eta^1-\eta^1$, the molecular dioxygen could be in cis−cis (labeled as CC), cis−trans (CT), or trans−trans (TT) position.

In Figure 5 are reported the optimized geometrical parameters for four structures. The bond lengths (in Å) and bond angles (in

Table 4. Theoretical Vibrational Frequencies (in cm^{-1}) for the Three Retained Geometries Calculated at the M06L/Aug-cc-pVTZ Level[a]

		ν_1	ν_2	ν_3	ν_4	ν_5	ν_6	ν_7	ν_8	ν_9	ν_{10}	ν_{11}	ν_{12}	ν_{13}	ν_{14}	ν_{15}
M06L	CT	7.0 (0.03)	28.5 (0.2)	100.4 (0.15)	130.6 (0)	157.5 (2.27)	193.9 (0.1)	207.1 (2.29)	231.8 (0.69)	289.3 (0.36)	409.7 (1.15)	414.4 (1.17)	891.1 (19.76)	953.8 (23.81)	1401.9 (100)	1449.7 (52.28)
	CC	36.2 (0.27)	69.2 (0.06)	136.7 (0)	144.8 (0.46)	176.3 (0.27)	189.8 (1.7)	206.1 (0.67)	206.6 (2.68)	312.2 (0.03)	417.4 (0.3)	418.9 (1.0)	879.5 (20.1)	956.4 (28.68)	1390.4 (100)	1442.4 (52.31)
	TT	75.3 (0)	78.9 (0.06)	79.5 (0.02)	134.5 (2.1)	152.5 (0)	183.5 (0.08)	209.1 (1.22)	241.1 (0.9)	269.2 (1.02)	374.2 (1.86)	433.2 (0.45)	884.5 (13.79)	945.6 (19.13)	1412.3 (100)	1455.0 (44.84)
TPSSh	CT	40.9 (0.1)	79.9 (0.04)	102.1 (0.06)	130.9 (0)	159.4 (2.17)	186.6 (0.06)	191.4 (3.06)	219.2 (1.25)	280.6 (0.42)	400.6 (1.87)	407.6 (1.41)	907.6 (18.92)	968.4 (18.71)	1355.9 (100)	1411.6 (47.04)
	CC	53.4 (0.17)	81.4 (0.02)	135.8 (0.07)	143 (0.21)	173.4 (0.52)	191.5 (1.98)	193 (1.03)	195.3 (3.22)	305.8 (0.02)	413.5 (1.36)	417.1 (0.76)	898.2 (19.87)	973.8 (21.76)	1337 (100)	1399.3 (47.04)
	TT	73 (0.05)	84.4 (0.05)	88.3 (0)	138.2 (0)	145 (2.15)	171.2 (0.08)	199.4 (1.59)	230.3 (1.88)	263.5 (0.96)	366.3 (2.79)	419.3 (0.59)	903.1 (14.2)	962.2 (15.52)	1370.2 (100)	1419.1 (42.0)

[a] Relative intensities are in parentheses.

dx.doi.org/10.1021/jp203943x |J. Phys. Chem. A 2011, 115, 9014–9021

Table 5. Comparison of Experimental and Calculated Frequencies (cm^{-1}) for the Cis−Trans Structure of CoO_6[a]

mode	$Co(^{16}O_2)_3$ frequencies		$Co(^{18}O_2)_3$ isotopic shifts		$Co(^{16}O_2)_n(^{18}O_2)_{3-n}$ isotopic shifts		$Co\ (^{16}O^{18}O)_n\ (^{16}O_2 + {}^{18}O_2)_{3-n}$ isotopic shifts	
	obsd	calcd	obsd	calcd	obsd	calcd	obsd	calcd
ν_5 (A′) wagging	147.6	157.5	−8.1	−8.1	−4	−4.7		
ν_7 (A′) CoO *cis*-stretch	166.6	207.1	−7.7	−11.2	−4.1	−3.5		
ν_{10}(A′) CoO a-bend	370.2	409.7	19.8	−21.8		−15.9		
					−17.8	−17.1		
ν_{11}(A′) CoO a-bend	377.8	414.4	−18.4	−21.2	−0.8	−0.7		
						−1.6		
ν_{12}(A′) OCoO s-stretch	797.8	891.1	−39.4	−44.1		0	−23	−27.9
						−44.1		
ν_{13}(A″)OCoO a-stretch	897.5	953.8	−35.1	−38.3		0	−14.3	−13.3
						−38.3		
ν_{14}(A′) O═O a-stretch	1331.3	1401.9	−74.5	−80.2		0	−21.4	−22.6
					−57	−59.2	−23.8	−24.5
						−59.3	−28.7	−29.3
					−65.8	−68	−29.9	−31.3
						−68	−31.1	−38.2
						−80.2	−36.2	−39.6
							−37.1	−40.8
							−37.7	−64.0
							−60.5	−64.5
							−67.7	−70.8
								−71.3
ν_{15}(A′) O═O s-stretch	1365.1	1449.7	−76.4	−83.1	−18.7	−22.7	−7	−9.6
					−9.4	−13.3		−9.9
						−82.9	−14.7	−16.7
						−22.8		−16.8
						−13.4	−36.8	−40.0
						0	−37.8	−40.8
							−38.6	−41.7
							−43.2	−49.8
							−45.8	−51.4
							−51.0	−56.8
							−53.1	−58.7

[a] For the isotopically mixed species, only the signals for species not containing only $^{16}O_2$ or $^{18}O_2$ are reported.

degrees) displayed in Figure 5 are for doublet state, while those of the quartet state are reported in parentheses.

The energetic results reported in Table 2 could be highlighted as follows:

1 All the sextet state structures are dissociative and evolve toward $OCoO(O_2) + O_2$.
2 Any $\eta^2-\eta^2$ structure converges toward a $\eta^1-\eta^2$ or $\eta^1-\eta^1$ structure, depending on the starting point.
3 In the doublet state, three $\eta^1-\eta^1$ structures, namely, CC, CT, and TT (Figure 5), are nearly isoenergetic and correspond to the ground state. Nevertheless, the CT structure is calculated slightly more stable, with the CC and TT structures found to be, respectively, only at 6 and 120 cm^{-1} higher in energy than the CT structure. We note that the binding energy of the $\eta^1-\eta^1$ CT doublet structure with respect to the $OCoO + 2O_2$ was found to be 11207 cm^{-1} (134 kJ/mol).
4 The corresponding CT, CC, and TT $\eta^1-\eta^1$ quartet states are found to be higher than the $\eta^1-\eta^1$ (CT) doublet state by 3185, 3744, and 4055 cm^{-1}, respectively.
5 The two $\eta^1-\eta^2$ structures (doublet and quartet states) have an intermediate energy with respect to both doublet and quartet states of the $\eta^1-\eta^1$ structures. However, the quartet $\eta^1-\eta^2$ structure is more stable than its doublet homologue. They are found to be at 1237 and 1801 cm^{-1} higher than the $\eta^1-\eta^1$ CT doublet state, respectively.
6 It is worth noting that all the $\eta^1-\eta^1$ doublets as well as the $\eta^1-\eta^2$ doublet and quartet states are strongly contaminated, indicating the presence of a strong left-right correlation in these compounds.

We are henceforth interested in the study of $\eta^1-\eta^1$ structures for the doublet states only, labeled CC, CT, and TT, because they are the most stable states and seem quasi-degenerate. However, only one of them corresponds to the experimentally observed structure. To check this result, the three structures have been optimized using nine different functionals with the 6-311+G(2d) basis-set. Only two functionals (M06L and OB95) predict the CT form as the most stable one as experimentally observed. The CC structure is calculated more stable for the five following functionals

dx.doi.org/10.1021/jp203943x |J. Phys. Chem. A 2011, 115, 9014–9021

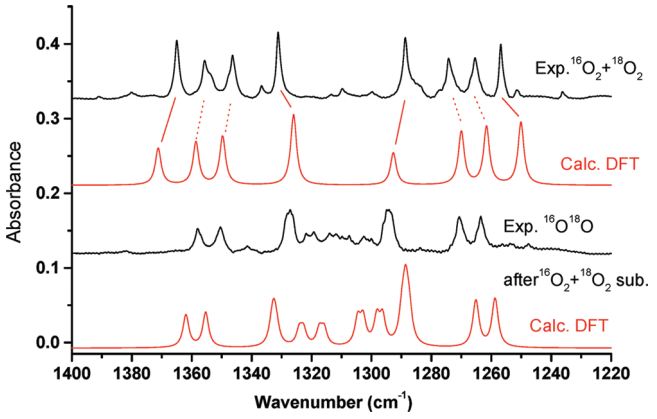

Figure 6. Comparison of experimental (black) and predicted (red) isotopic patterns for $^{16}O_2$ + $^{18}O_2$ and $^{16}O^{18}O$-labeled CoO_6 species. The calculated frequencies are rescaled by 0.95 to provide pictorial comparison.

(TPSSTPSS, BPW91, PBEPBE, BB95, and mPWB95), but for the two last ones (TPSSh and OPBE), the TT form is predicted the more stable.

As reported in Table 3, for the energetic results, the three $\eta^1-\eta^1$ doublet states all show a high spin contamination, due to the presence of a strong nondynamic correlation, whatever the functional used. The same trend is observed when changing the basis set (Aug-cc-pVTZ) using the most successful functionals, M06L for instance.

Vibrational Predictions and Analysis. For the vibrational study, we used the M06L as a local density functional and TPSSh, as recommended by Jensen,[38] with Aug-cc-pVTZ. M06L, the most recent *meta*-GGA method, provides better performances for metallic systems. It has been shown that calculations are tens or hundreds of times faster with local density functionals than with nonlocal ones.[39,40] Furthermore, over the nine functionals used here, only the M06L gives results in good agreement with the experimentally observed ones: the stable species must have two nonequivalent dioxygen, such as is the case in the $\eta^1-\eta^1$ CT structure. Furthermore, this system presents a strong nondynamic correlation that should be well described with a local and nonhybrid functional, such as an M06L one.

Following the recommendation of Jensen and co-workers, we also use the TPSSh functional[38] in parallel to the M06 vibrational analysis. All the calculated vibrational frequencies for the three doublet $\eta^1-\eta^1$ structures at the M06L/Aug-cc-pVTZ and TPSSh/Aug-cc-pVTZ levels are reported in Table 4. To facilitate comparisons, the vibrational modes have been numbered in increasing energy order, regardless of symmetry.

The calculated frequencies are overestimated by 5 to 10% in comparison with the experimental ones, this might be due to systematic methodological effects, and certainly also to the neglect of anharmonicity and possible environmental effects (Table 5). Nevertheless the agreement is within the usual range, and this study enables an analysis of the isotopic effects. First the $^{16}O_2/^{18}O_2$ shifts are in line with assignment of the four low frequency bands to a wagging motion of the CoO_2 group and Co−OO bending and stretching modes. The two cobalt dioxide asymmetric and symmetrical stretching modes near 900 and 800 cm^{-1} are qualitatively well reproduced by the calculation, as the mode ordering and coupling of the two Co═O coordinates match the experimental results for the ^{16}O $Co^{18}O$ isotope. Note that the coupling of the Co═O with the superoxide vibration is calculated to be much smaller than the line widths, explaining the absence of extra signals for the O═Co═O $(^{18}O_2)_2$ or ^{18}O═Co═^{18}O $(O_2)_2$, for example. The reproduction of the vibrational isotopic pattern produced by the coupling between the two O═O coordinates of slightly different energies and with the corresponding Co−O_2 bonds is also qualitatively satisfying. This is illustrated in Figure 6, the comparison between the observed isotopic pattern for $^{16}O^{18}O$-containing species and that which can be derived from the calculations, after rescaling the predicted frequencies by 0.95 to facilitate pictorial comparisons. One can note that the model slightly overestimates the coupling between the two superoxide groups, which results in an overestimation of the intensity of the lower of the two O═O stretching modes, as well as too large splittings between the two components of the O═Co═O $(^{18}O_2)(^{16}O_2)$ or O═Co═O $(^{18}O^{16}O)_2$. This should be improved in a multideterminental calculation, but the main trends are there.

Comparison with Other Systems. The CoO_6 species observed here is quite unique inasmuch as it contains a Co center in an unusually large formal oxidation number, as well as in its structure. Other systems of MO_6 stoichiometry have been evidenced and described in the case of Cr or Cu atoms, but in either cases, the structure is markedly different. For the CrO_6 species all three dioxygen ligands bind in a η^2-side on structure,[36] while for CuO_6, which contains two η^1-superoxo groups as CoO_6, the Cu center does not form a dioxide group.[37] Both species are thus prone to further transformation. The specificity of the Co center lies in its ability to form labile metal-superoxide bonds on a robust cobalt dioxide groups and constitutes a test case for reversible dioxygen fixation.

CONCLUSIONS

In this paper, we report new experimental and theoretical data on the complexation of oxygen molecules by CoO_2 to form a CoO_6 product, isolated in argon and neon matrices. Experimental data are obtained using IR absorption spectroscopy, resulting in the detection of eight fundamental bands. Vibrational analysis based on isotopic effects reveals unambiguously a nonsymmetrical structure with nonequivalent O atoms in the CoO_6 molecule, best described as $OCoO(\eta^1\text{-}O_2)_2$, a disuperoxo cobalt dioxide species.

Calculations are presented using the M06L/Aug-cc-pVTZ model within the BS-UDFT formalism to investigate the electronic and geometrical structure. The predicted ground state is an open shell doublet state with a C_s symmetry geometrical structure, with two slightly nonequivalent superoxo groups in a cis−trans configuration. More symmetrical structures, corresponding to states with slightly different C_{2v} configurations lie very close in energy. Quartet states are calculated much higher in energy and sextet states unbound with respect to $CoO_2(O_2)$ + O_2. The model is used to predict observable spectroscopic properties in good agreement with observation. These DFT-based calculations are then used to provide a realistic proposal for the reaction pathway. The $CoO_2(O_2)$ + O_2 complexation reaction is found to proceed spontaneously at 9 K in the dark and is calculated without energy barrier and exothermic by more than 30 kJ/mol. It is thus shown to be the main formation pathway under these conditions.

AUTHOR INFORMATION

Corresponding Author

*E-mail: esmail.alikhani@upmc.fr; laurent.manceron@upmc.fr.

REFERENCES

(1) Vaska, L. T. *Acc. Chem. Res.* **1976**, *9*, 175.
(2) Frenking, G. *Coord. Chem. Rev.* **2000**, *100*, 717.
(3) Li, G. Q.; Govind, R. *Ind. Eng. Chem. Res.* **1994**, *33*, 755.
(4) Niederhoffer, E. C.; Timmons, J. H.; Martell, A. E. *Chem. Rev.* **1994**, *84*, 137.
(5) Hutson, N. D.; Yang, R. D. *Ind. Eng. Chem. Res.* **2000**, *39*, 2252.
(6) Boscola, E.J. J. *Aircraft* **1974**, *11*, 444.
(7) Aducci, A. J. *CHEMTECH* **1975**, *6*, 575.
(8) Jones, R. D.; Summerville, D. A.; Basolo, F. *Chem. Rev.* **1979**, *79*, 139.
(9) Chen, D.; Martell, A. E.; Sun, Y. *Inorg. Chem.* **1987**, *26*, 1026.
(10) Rybak-Akimova, E. V.; Marek., K.; Masarwa, M.; Busch, D. H. *Inorg. Chim. Acta* **1998**, *270*, 151.
(11) Gong, Y.; Zhou, M.; Andrews, L. *Chem. Rev.* **2009**, *109*, 6765.
(12) Chertihin, G. V.; Citra, A.; Andrews, L.; Bauschlicher, C. W., Jr. *J. Phys. Chem. A* **1997**, *101*, 8793.
(13) Danset, D.; Alikhani, M. E.; Manceron, L. *J. Phys. Chem. A* **2005**, *109*, 97.
(14) Danset, D.; Alikhani, M. E.; Manceron, L. *J. Phys. Chem. A* **2005**, *109*, 105.
(15) Danset, D.; Manceron, L. *J. Phys. Chem. A* **2003**, *107*, 11324.
(16) Becke., A. D. *Phys. Rev. A* **1988**, *38*, 3098.
(17) Perdew, J. P. In *Electronic Structure of Solids '91*; Ziesche, P., Eschrig, H., Eds.; Akademie Verlag: Berlin, 1991; p 11.
(18) Hoe, W.-M.; Cohen., A. J.; Handy., N. C. *Chem. Phys. Lett.* **2001**, *341*, 319.
(19) Perdew, J. P.; Burke, K.; Ernzerhof, M. *Phys. Rev. Lett.* **1996**, *77*, 3865.
(20) Tao, J.; Perdew, J. P.; Staroverov, V. N.; Scuseria, G. S. *Phys. Rev. Lett.* **2003**, *91*, 146401.
(21) Zhao, Y.; Truhlar, D. G. *J. Chem. Phys.* **2006**, *125*, 194101.
(22) Zhao, Y.; Truhlar, D. G. *Theor. Chem. Acc.* **2008**, *120*, 215.
(23) Becke, A. D. *J. Chem. Phys.* **1996**, *104*, 1040.
(24) Adamo, C.; Barone, V. *J. Chem. Phys.* **1998**, *108*, 664.
(25) McLean, A. D.; Chandler, G. S. *J. Chem. Phys.* **1980**, *72*, 5639.
(26) Dunning, T. H., Jr. *J. Chem. Phys.* **1989**, *90*, 1007.
(27) Ovchinnikov, A. A.; Labanowski, J. K. *Phys. Rev. A: At. Mol. Opt. Phys.* **1996**, *53*, 3946.
(28) Ciofini, I.; Daul, C. A. *Coord. Chem. Rev.* **2003**, *187*, 238.
(29) Himmel, H. J.; Hübner, O.; Bischoff, F.; Klopper, W.; Manceron, L. *Phys. Chem. Chem. Phys.* **2006**, *8*, 2000.
(30) Staemmler, V.; Reinhardt, P.; Allouti, F.; Alikhani, M. E. *Chem. Phys.* **2008**, *349*, 83.
(31) Souvi, S. O.; Berkaïne, N.; Alikhani, M. E.; Manceron, L. *Phys. Chem. Chem. Phys.* **2009**, *11*, 9831.
(32) Ould Souvi, S.; Danset, D.; Manceron, L.; Alikhani, M. E. *J. Phys. Chem.* **2010**, *114*, 11399.
(33) Frisch, M. J.; Trucks, G. W.; Schlegel, H. B.; Scuseria, G. E.; Robb, M. A.; Cheeseman, J. R.; Scalmani, G. ; Barone, V.; Mennucci, B.; Petersson, G. A.; Nakatsuji, H.; Caricato, M.; Li, X.; Hratchian, H. P.; Izmaylov, A. F.; Bloino, J.; Zheng, G.; Sonnenberg, J. L.; Hada, M; Ehara, M.; Toyota, K.; Fukuda, R. ; Hasegawa, J.; Ishida, M.; Nakajima, T.; Honda, Y.; Kitao, O.; Nakai, H.; Vreven, T.; Montgomery, J. A., Jr.; Peralta, J. E.; Ogliaro, F.; Bearpark, M.; Heyd, J. J.; Brothers, E.; Kudin, K. N.; Staroverov, V. N.; Kobayashi, R.; Normand, J.; Raghavachari, K.; Rendell, A.; Burant, J. C.; Iyengar, S. S.; Tomasi, J.; Cossi, M.; Rega, N.; Millam, J. M.; Klene, M.; Knox, J. E.; Cross, J. B; Bakken, V.; Adamo, C.; Jaramillo, J.; Gomperts, R.; Stratmann, R. E; Yazyev, O.; Austin, A. J.; Cammi, R.; Pomelli, C.; Ochterski, J. W.; Martin, R. L.; Morokuma, K.; Zakrzewski, V. G.; Voth, G. A.; Salvador, P.; Dannenberg, J. J.; Dapprich, S.; Daniels, A. D.; Farkas, O.; Foresman, J. B.; Ortiz, J. V.; Cioslowski, J. *Gaussian 09*, Revision A.02; Gaussian, Inc.: Wallingford, CT. 2009.
(34) Danset, D.; Manceron, L. *Phys. Chem. Chem. Phys.* **2005**, *7*, 583.
(35) Danset, D.; Manceron, L. *Phys. Chem. Chem. Phys.* **2004**, *6*, 3928.
(36) Gong, Y.; Wang, G.; Zhou, M. *J. Phys. Chem. A* **2009**, *113*, 5355.
(37) Zhao, Y. Y.; Su, J.; Gong, Y.; Li, J.; Zhou, M. *J. Phys. Chem. A* **2008**, *112*, 8606.
(38) Jensen, K. P.; Cirera, J. *J. Phys. Chem. A* **2009**, *113*, 10033.
(39) Te Velde, G.; Bickelhaupt, F. M.; Baerends, E. J.; Fonseca Guerra, C.; Van Gisbergen, S. J. A.; Snijders, J. G.; Ziegler, T. *J. Comput. Chem.* **2001**, *22*, 931.
(40) Füsti-Molnár, L.; Pulay, P. *THEOCHEM* **2003**, *25*, 666.